Magnetic graphene TiO_2-based photocatalyst for the removal of pollutants of emerging concern in water by simulated sunlight aided photocatalytic ozonation

Ana M. Chávez[1,2], Rafael R. Solís[3*], Fernando J. Beltrán[1,2]

[1]Departamento de Ingeniería Química y Química Física, Facultad de Ciencias, Universidad de Extremadura, Avda. Elvas s/n, 06071 Badajoz (Spain)

[2]Instituto Universitario del Agua, Cambio Climático y Sostenibilidad (IACYS), Universidad de Extremadura, Avda. de la Investigación s/n, 06071 Badajoz (Spain)

[3]Department Chemical & Environmental Engineering, College of Engineering & Environmental Science (CEAS), Engineering Research Centre (ERC), University of Cincinnati, Cincinnati OH 45221-0012 (USA)

*To whom correspondence should be addressed: Rafael Rodríguez Solís (rodrigr2@ucmail.uc.edu)

Abstract

Magnetite and titania have been supported onto graphene for the photocatalytic ozonation removal of aqueous micropollutants. Titania and magnetite were successfully attached to graphene nanoparticles keeping with a reasonable separation and photocatalytic activity. Although the presence of graphene did not enhance the photoactivity of bare titania, graphene acted as a good support of magnetite nanoparticles and removed the leaching of iron, a problem observed with the graphene free composite. The synthesized photocatalysts were characterized by diverse techniques. The efficiency of the processes involving ozone was assessed by different tools such as $HO^{\bullet}$ exposure vs time, R_{CT} and $R_{HO^{\bullet},O3}$ ratios. Photocatalytic ozonation was the most efficient for the removal of the target compound and mineralization. No loss of activity was registered after reusing or appreciable iron leaching. Finally, the catalyst was also tested in a real secondary effluent from a wastewater treatment plant containing ten micropollutants of emerging concern.

Keywords: magnetic graphene, titania, photocatalytic ozonation, solar light, water treatment

1. INTRODUCTION

The high standard of life reached by current Society demands the use of a huge number of organic substances that are still under research and development every day. However, the concern related to the presence of these organics in the Environment is raising among the research community due to the harmful properties and their impact in the natural ecosystems [1]. Concretely, Contaminants of Emerging Concern (CECs) are organic micropollutants, i.e. reported at very low concentration, from diverse families of organics: pharmaceuticals, personal care products, plasticizers, perfluorochemicals, food additives, legal and illegal drugs, pesticides, etc. [2–4]; that have been detected in diverse aqueous ecosystems for the last decades. Furthermore, these substances generate some stable degradation products named as metabolites. The acute toxicity of CECs is not always alarming as the concentration they are reported at is below $\mu g\ L^{-1}$, commonly in the $ng\ L^{-1}$ range. In addition, their interaction with human life and the Environment is not well understood. No studies of how they affect the life cycle in the long term are available [5]. Nevertheless, some groups of these substances do generate a concern impact in the short term. For example, the presence of antibiotics in the Environment is making microbes to be more resilient as they adapt themselves against the antibacterial properties [6,7].

Although drinking water treatment plants generally are designed to remove specific organic pollutants when required, conventional Urban WasteWater Treatment Plants (UWWTPs) do not consider specific stages for that purpose. This makes UWWTPs to be a hotspot of CECs release into aquatic ecosystems [8,9]. Thus, new technologies to face the problematic of CECs are needed.

Advanced Oxidation Processes (AOPs) have demonstrated to be efficient in the oxidation of almost all kind of organics in water [10–12]. AOPs rely on the production of hydroxyl radicals in enough concentration to oxidize organics, approaching in some cases

high mineralization extent as the oxidation is focused on the production of carbon dioxide and inorganic anions. Ozone is a versatile and moderate oxidant that does not produce residues when used in water treatment. Ozone can react, first, unselectively by direct attack of the O_3 molecule to e.g. unsaturated bonds or aromatic rings; and secondly, by triggering a decomposition mechanism into hydroxyl radical as the main oxidant species. However, ozonation by itself poses low potential of mineralization [13]. That is why different technologies that enhance the decomposition of aqueous ozone into $HO^{\bullet}$ have gained the attention of researchers. Among all envisaged technologies, photocatalytic ozonation is one of the most powerful due to the high mineralization extent capability [14–18]. That means, that not only the targeted compounds are oxidized, but also the intermediates and a great extent of the final oxidation products such as organic acids.

Titanium dioxide, activated with radiation below 387 nm [19], has led the study of photocatalytic ozonation processes due to its high stability, low toxicity and price, if compared to other photoactive catalysts. Although the solid frequently has been displayed in slurry reactors; this disposition lacks interest since further recovery of the catalyst is required, which is economically low attractive. The immobilization of the solid is one strategy trying to deal with this problem [20], even though some radiation adsorption effectiveness is reduced if compared to slurry setup [21]. Alternatively, magnetization of the catalyst has been proved to be an efficient strategy to take advantage of the high radiation adsorption in slurry disposition and easy recovery by applying and external magnetic field after use [22,23]. In this sense, for TiO_2 photocatalysis, some magnetic solids containing Fe_3O_4 with high photocatalytic activity have been proposed [24]. Different high specific surface area supports have been previously tested for magnetic-based TiO_2 using carbonaceous materials such as activated carbon [25,26] or multi-walled carbon nanotubes [27,28]. Graphene, which is defined a single monolayer of hexagonal

carbon, is also a high surface material with high delocalization of π electrons, which confers on it promising properties as nano-adsorbent [29] and nano-catalyst [30–33].

This work reports the study of magnetic titania photocatalysts using graphene as support for the photocatalytic ozonation process, under solar simulated radiation, of aqueous contaminants of emerging concern. Different photocatalysts varying the ratios of the photocatalytic specie (TiO_2), magnetic specie (Fe_3O_4) and support (graphene) have been tested using preliminary studies in ultrapure water with cotinine, which is recalcitrant to oxidation metabolite of nicotine [34], frequently reported in wastewater effluents [35–38]. Different techniques have been used for the characterization of the synthesized materials (i.e. SEM-EDX, TEM, XRD, FTIR, Raman, N_2 isotherm, XPS, XRF, DRS-Vis, SQUID…) in order to analyze the influence of superficial and textural properties on the photocatalytic activity. The material with higher activity was tested for stability in consecutive recycling and iron leaching was only observed in graphene free composite at values well above the detection limit. Finally, deeper testing for oxidation of a mixture of CECs (bezafibrate, caffeine, ciprofloxacin, clofibric acid, cotinine, DEET, ibuprofen, metoprolol, sulfamethoxazole and tritosulfuron) at low concentration and dissolved in a real UWW effluent is accomplished.

2. EXPERIMENTAL

2.1. Chemicals and materials

Cotinine analytical standard (CTN, $C_{10}H_{12}N_2O$, CAS: 486-56-6, ≥98%), bezafibrate (BZF, $C_{19}H_{20}ClNO_4$, CAS: 41859-67, ≥98%), caffeine (CAF, $C_8H_{10}N_4O_2$, CAS: 58-08-2, ≥99%), clofibric acid (CLO, $ClC_6H_4OC(CH_3)_2CO_2H$, CAS: 882-09-07, 97%), ibuprofen sodium salt (IBP, $C_{13}H_{17}O_2Na$, CAS: 31121-93-4, ≥98%), metoprolol tartrate (MTP, $(C_{15}H_{25}NO_3)_2{\cdot}C_4H_6O_6$, 56392-17-7, 99%), N,N-diethyl-m-toluamide (DEET, $C_{12}H_{17}NO$, 134-62-3, 97%), sulfamethoxazole (SMX, $C_{10}H_{11}N_3O_3S$, 723-46-6, ≥98%)

and tritosulfuron (TSF, $C_{13}H_9F_6N_5O_4S$,142469-14-5, ≥98%) were acquired from Sigma-Aldrich®. Ciprofloxacin (CPR, $C_{17}H_{18}FN_3O_3$, CAS:85721-33-1, 98%) was supplied by Acros Organics®.

For catalyst synthesis, commercial xGnP® graphene nanoplatelets from Sigma-Aldrich® was used (particle size < 2µm, thickness few nm, specific surface area 750 m^2 g^{-1}). Titanium (IV) *iso*-propoxide (Sigma-Aldrich®) and pure *iso*-propanol (Panreac®) were used in the TiO_2 solvothermal method synthesis. All chemicals were used as-obtained without any further purification.

The rest of the chemicals used for analytical purposes were analytical grade and purchased from Panreac®. HPLC-grade acetonitrile (Panreac®) was used in liquid chromatography. Ultrapure Milli-Q® from an Integral 5 system (resistivity 18.2 MΩ cm) was used for the preparation of all the solutions. Urban WasteWater (UWW) coming from a secondary clarifier after biological treatment was collected from the local WasteWater Treatment Plant (WWTP) of the city of Badajoz in the spring of 2019 (capacity for 160,000 equivalent inhabitants), filtered with paper filters (>11 µm) and stored at -4 ºC until further use. Table 1 summarizes the main characterization parameters of the UWW.

Table 1. Characterization parameters of the UWW effluent

Parameter (units)	**Mean value ± error**
pH	8.4±0.1
Conductivity (µS cm^{-1})	960
Turbidity (NTU)	5.2
Total Organic Carbon, TOC (mg L^{-1})	20.2 ± 0.7
Inorganic Carbon, IC (mg L^{-1})	58 ± 2
Chloride (mg L^{-1})	104 ± 9
Nitrate (mg L^{-1})	0.41 ± 0.02
Phosphate (mg L^{-1})	0.24 ± 0.02
Sulfate (mg L^{-1})	60 ± 3

2.2. Catalyst synthesis and characterization

The synthesis of magnetic graphene-TiO_2 based photocatalysts was adapted from literature [39]. Briefly, the procedure was as follows. Firstly, magnetite nanoparticles were obtained by simultaneous co-precipitation of Fe^{3+} and Fe^{2+} at the same molar ratio under alkaline conditions. Thus, 20 mmol of $FeCl_3 \cdot 6H_2O$ and 20 mmol of $FeSO_4 \cdot 7H_2O$ were dissolved in 200 mL of ultrapure water under N_2 bubbling and magnetic stirring. Solution pH was raised until the value of ~9.0 by dropwise of concentrated aqueous NH_3 solution. The magnetic particles were washed with water under stirring, recovering the particles with the help of a magnet. The washed solid was dried overnight at 80ºC. Secondly, magnetic graphene was prepared by sonicating a certain amount of the previously obtained magnetite and commercial graphene in 200 mL of *iso*-propanol. Different weight ratios of magnetite:graphene (X:1) were considered, labeling them as MGX. Thirdly, TiO_2 was incorporated to the magnetic-graphene substrate by solvothermal method. For that purpose, 10 mL of titanium (IV) *iso*-propoxide were dissolved in 50 mL of *iso*-propanol and a desired amount of MGX was added to the solution. The catalyst was labeled as Y-MGX-Ti where Y stands the mass percentage of MGX in comparison to the theoretical TiO_2 incorporated in the process. Precipitation of titanium was accomplished by adding 5 mL of ultrapure water and the solution was transferred to a 200 mL autoclave. Thermal treatment was undergone at 180ºC during 16 h. The final solid was washed with ethanol and ultrapure water several times. Finally, solid was dried under vacuum at 80ºC and kept overnight at 80ºC.

Graphene percentage was thermogravimetrically obtained by calcination at 800ºC. The ratio Fe/Ti was quantified by Wavelength Dispersive X Ray Fluorescence (WDXRF) in a S8 TIGER® device (Bruker), equipped with Rh X-ray source (4 kW).

146 Morphology of the solid was studied by Scanning Electron Microscopy (SEM) in a
147 QUANTA 3D FEG (FEI Company) device, equipped with BSED (Backscattered
148 Electron Diffraction) and EDX (Energy Dispersive X-ray) analysis.

149 N_2 adsorption isotherm technique was conducted to evaluate the textural properties,
150 using a Quadrasorb EvoTM apparatus (Quantachrome Instruments). Aautosorb IQ-c
151 software was used to obtain BET surface area ($0.05<p/p0<0.35$), as well as analysis of
152 external surface area and micropore volume distribution. Samples were previously
153 outgassed at 150ºC for 12 h under vacuum.

154 Microcrystalline structure was analyzed by X-Ray Diffraction (XRD), performed in a
155 D8 ADVANCE device (Bruker) equipped with Vário-1 Ge111 monochromator (Cu $K\alpha_1$,
156 radiation 1.5406 Å), registering within an angle range (2θ) 5-70º.

157 Raman spectra were obtained in a Nicolet^{TM} Almega XR Dispersive Raman
158 Spectrometer (Thermo Scientific^{TM}) provided with a laser at 633 nm. Fourier
159 Transformed InfraRed (FTIR) spectra were registered in a Nicolet^{TM} iS10 FTIR
160 spectrometer (Thermo Scientific^{TM}) in the range 7800-350 cm^{-1}.

161 Superficial oxidation states and surface oxygenated groups were analyzed by X-Ray
162 Photoelectron Spectroscopy (XPS) in a Kratos Axis Ultra DLD device operating with
163 monochromatic Al Kα radiation (1486.6 eV) and a selected X-ray power of 150 W.
164 Spectra were corrected to 284.8 eV for C-C bounding in C 1s peak. The deconvolution of
165 the peaks was carried out with help of XPSPeak 4.1 software, adopting a Shirley type
166 background correction.

167 Optical properties were studied in a Diffuse Reflectance UV-vis spectrophotometer
168 (DR-UV-vis), UV-vis-NIR Cary-5000 (Varian Technologies), equipped with integrating
169 sphere device. Band gap was calculated following Tauc's method [40].

Magnetic properties were measured using a 7 Tesla Quantum Design MPMS XL Superconducting Quantum Interference Device (SQUID). The magnetic moment, M, was measured as function of applied magnetic field (from 0 to 7 T) at room temperature (300 K).

2.3. Photocatalytic ozonation tests

Photocatalytic tests were carried out in a simulated solar box SUNTEST CPS+ (Atlas) equipped with Xe arc lamp and emitting radiation at >300 nm. A glass borosilicate spherical reactor, with 500 mL of water solution, was placed in the center of the solar simulator and kept under magnetic stirring. Pure O_2 or O_2-O_3 gas mixture, with ozone generated in a Anseros COM-AD-01 apparatus, was bubbled at a rate of 30 L h^{-1}, containing 10 mg O_3 L^{-1} (when needed). Ozone concentration in the gas phase was continuously monitored by means of an Anseros GM device (spectrophotometric measurement at 254 nm), connected to the gas outlet/inlet of the reactor. A detailed experimental setup scheme can be checked in previous works [41].

Experiments started with a 30 min adsorption period, when required, to ensure the adsorption equilibria on the catalyst surface. Photocatalytic ozonation started by simultaneously application of radiation and ozone bubbling. In experiments in which radiation was not necessary, for temperature profiles comparison, radiation was supplied but the reactor was prevented from radiation by covering it with aluminum foil. At different times aqueous samples were withdrawn, removing residual dissolved ozone by bubbling air and filtering the catalyst with Millex®-HA syringe filters (0.45 μm, Millipore®), when required.

193 **2.4. Analysis of aqueous samples**

194 The concentration of organic pollutants was analyzed by HPLC in a UFLC Shimadzu
195 Prominence LC-20AD device equipped with Diode-Array detection. The column used
196 for the chromatographic separation was a core-shell Kinetex® (C18, 2.6 μm, 2.1x30 cm),
197 kept at 30ºC. For individual analysis of cotinine, a mixture A:B=5:95 acetonitrile:
198 acidified water (0.1% H_3PO_4), was pumped at a rate of 0.5 mL min^{-1}. Quantification was
199 conducted at 259 nm. The method followed for the mixture of the contaminants was a
200 gradient, with the same flow rate, starting with A:B=5:95 during 5 min, thereafter the A
201 proportion was raised until 95:5 in 15 min, and hold during 1 min to go back to the initial
202 conditions in 9 min. Detailed information on quantification wavelength and retention
203 times are provided in Table S1.

204 Dissolved ozone in the aqueous phase was determined by the colorimetric method
205 based on the discoloration of indigo trisulfonate [42].

206 Total Organic and Inorganic Carbon was quantified in a Shimadzu® TOC-V_{CSH}
207 coupled to ASI-V automatic injector.

208 Short organic acids (acetic, propionic, formic and oxalic acid) and inorganic anions
209 (chloride, nitrate, phosphate and sulfate) were analyzed by ionic chromatography in a
210 Methrom® 881 Compact IC pro equipped with chemical suppression. The mobile phase
211 program was a gradient of 0.7 mL min^{-1} of Na_2CO_3 from 0.6 mM to 14.6 mM in 50 min,
212 with 10 min of equilibration.

213 The released iron into solution was quantified spectrophotometrically as total iron by
214 ferrozine method (Spectroquant®, Merck).

3. RESULTS AND DISCUSSION

3.1. Characterization of the photocatalysts

The composition of the synthetized photocatalysts were studied by combining different techniques. The carbon percentage was calculated by calcination and the ratio of Fe:Ti by WDXRF analysis. Table 2 summarizes the results. As shown, the proportion of MG1 was close to 1:1. The percentage of the incorporated titania was slightly lower to the expected, but matching quite well with the theoretical desired. However, the amount of magnetite was generally inferior to a ratio 1:1 graphene magnetite in Y-MG1-Ti solids. There was a clear loss of magnetic particles during the washing step of the catalyst preparation. This latter aspect is even more obvious when the proportion graphene-magnetite was increased two and three times in the 10-MG2-Ti and 10-MG3-Ti. The loss of magnetite particles during the synthesis process could be attributed to a lack of real affixing during the thermal treatment in the solvothermal method.

The morphology of the photocatalytic particles was also studied by SEM technique. From the micrographs in Fig. S1, a wide variety of particle sizes within 10 and 50 μm was appreciated. An EDX mapping confirmed the presence of titanium and iron on the surface, as well as verified the distribution of magnetite and titania particles. The superficial composition estimated by EDX was in good agreement with the composition calculated by WDXRF, as shown in Table 2. From the distribution of carbon in EDX scanning, it can be observed that graphene acts as support of titania and magnetite particles.

Textural properties were analyzed by N_2 adsorption isotherm (graphs available in Fig. S2). The raw commercial graphene presented a BET specific area of 669 $m^2\ g^{-1}$, which is close to the value available from the manufacturer (750 $m^2\ g^{-1}$). The solvothermal prepared TiO_2 had a good surface area, 146 $m^2\ g^{-1}$, if compared to other nanosynthesized

240 titania. The addition of magnetic graphene support did not affect significantly the final
241 surface area, being in all the cases in between 150-200 m^2 g^{-1}. Nevertheless, there is a
242 correlation of the amount of graphene, e.g. with the highest graphene:magnetite ratio, and
243 the increase of the superficial area in the Y-MG1-Ti photocatalysts. Additionally, the pore
244 volume and its distribution (see Fig. S2) was analyzed by Density Functional Theory
245 (DFT), concluding that graphene support was the most porous material. All the
246 photocatalysts had similar pore volume (in the proximity of 0.320-0.374 cm^3 g^{-1}) and
247 similar pore distribution as it is highly influenced by the predominant content of titania.

Table 2. Elemental, superficial, optical and magnetic properties of the synthesized photocatalysts

Catalyst	Composition (weight, %)			Textural properties		Optical properties	Magnetic properties	
	C	Fe_3O_4	TiO_2	BET area ($m^2\ g^{-1}$)	Pore volume[3] ($cm^3\ g^{-1}$)	Band gap (eV)	Saturation Moment (emu g^{-1})	Theoretical saturation moment[4] (emu g^{-1})
Graphene	100	-	-	669	0.856	n.m.	n.m.	n.m.
MG1	53.6	45.0	-	56	0.516	n.m.	34.5	31.5
10-MG1-Ti	9.9[1]/ 6.5[2]	4.2[1]/ 4.5[2]	85.9[1]/ 88.8[2]	171	0.374	3.15	2.74	2.94
10-MG1-Ti re	2.1	4.4	92.6	142	0.322	n.m.	n.m.	n.m.
20-MG1-Ti	14.1[1]/ 9.5[2]	8.5[1]/ 9.0[2]	77.1[1]/ 81.5[2]	178	0.313	3.15	5.53	5.95
30-MG1-Ti	17.6[1]/ 14.3[2]	13.2[1]/ 12.8[2]	69.2[1]/ 72.9[2]	200	0.352	3.15	8.89	9.24
10-MG2-Ti	10.7	5.3	84.0	146	0.379	3.15	3.72	3.71
10-MG3-Ti	7.5	6.8	85.7	150	0.327	3.05	4.55	4.76
TiO_2	-	-	100.0	146	0.320	3.21	n.m.	n.m.

[1]Carbon thermogravimetrically quantified (calcination 800ºC). Magnetite and titania by WDXRF

[2]Measured by EDX analysis in SEM

[3]Obtained through Density Functional Theory (DFT) methodology

[4]Calculated according to the Fe_3O_4 composition and the saturation magnetization measured for pure Fe_3O_4 (70 emu g^{-1})

n.m. not measured

The crystalline composition of the different photocatalysts was qualitatively studied by X-ray Diffraction (XRD) technique. Fig. 1 depicts diverse diffractograms of some studied photocatalysts. Graphene XRD pattern was characterized by the presence of hexagonal graphitic peaks, i.e. mean peak at 26.7º and residual at 44.3º. After incorporating magnetite to obtain MG1, diverse peaks of cubic magnetite were observed, the most important located at 35.5º (minor peaks 30.1, 43.1, 53.7, 54.8 and 62.6º). Moreover, MG1 showed a small contribution of graphene peak (26º). The synthesized bare titania was also analyzed, confirming the presence of anatase with a main peak located at 25.2º (minor peaks at 37.7, 47.8, 53.7 54.8 and 62.4º). The XRD diffractogram of 10-MG1-Ti is characterized by the presence of the peaks of anatase, whose relative intensity was higher than magnetite, i.e. only the peak at 35.5º of cubic magnetite was appreciated. This peak increased as the proportion of MG1 was raised. Therefore, the presence of anatase and magnetite was confirmed in all Y-MGX-Ti photocatalysts, showing a relatively increase in the magnetite peak (i.e. 35.5º) when its proportion was increased. The presence of graphene in Y-MGX-Ti was not possible to confirm by this technique due to the higher relative intensity of anatase peak.

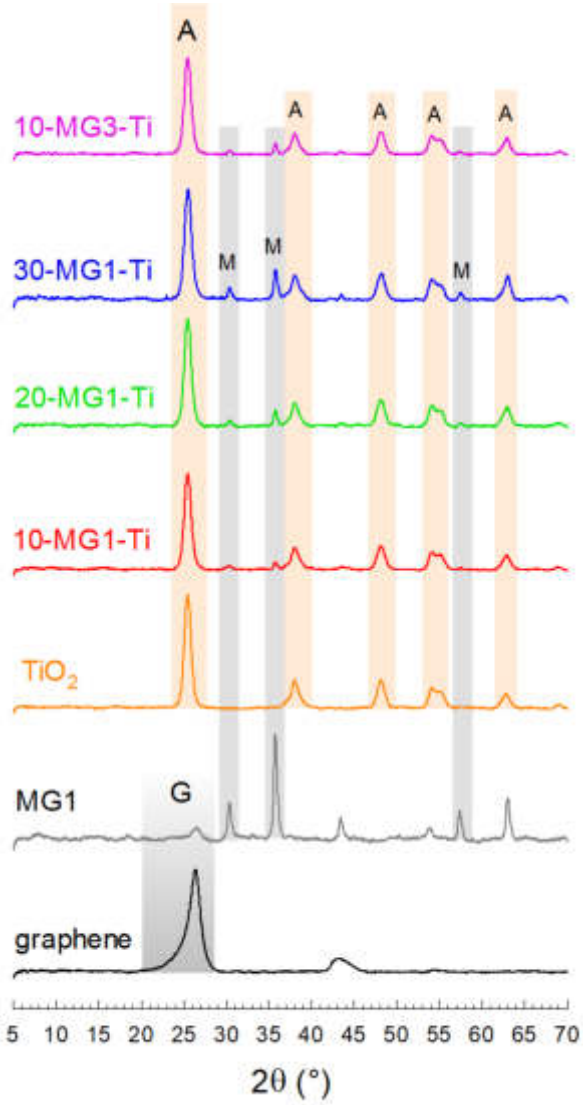

Figure 1. XRD pattern of Y-MGX-Ti photocatalysts

Thus, the presence of graphene was confirmed by Raman spectroscopy for the 10-MG1-Ti photocatalyst, see Fig. S3A. Raman patterns for titania, magnetite and graphene were also accomplished for comparison purposes. Particular information can be extracted from the Raman pattern of graphene in which three peaks are usually observed. The peak around 1350 cm^{-1} (D) is referred to disordered carbon, the G peak at *ca.* 1580 cm^{-1} is attributed to the hexagonal carbon present in graphene and the 2D-band, which gives information of the stacking order of graphene layers. The thickness of graphene nanoplatelets can be estimated by the relative intensity of 2D and G peak. A value up to 2 has been reported in the literature for monolayer graphene [55]. The Raman pattern for

the commercial graphene showed that I_{2D}/I_G=2.4. Alternatively, the Full Width at Half Maximum (FWHM) for 2D peak has also been studied for graphene materials of different layers [56]. A value of 25.6 cm^{-1} was estimated in this study, which coincides with the proposed value for monolayer graphene (FWHM=26 cm^{-1} [56]).

Additionally, Fourier Transform InfraRed spectroscopy (FTIR) was tested to evaluate the presence of oxygenated superficial groups (Fig. S3B). A wide band at *ca.* 3400 cm^{-1}, attributed to the stretching vibration of the hydroxyl group was observed in all the solids analyzed which qualitative justified the presence of coordinated –OH surface groups or molecules of H_2O adsorbed. Hydroxylated groups also present a deformed vibration at around 1600 cm^{-1}. It is also observed a peak at around 1400 cm^{-1} that usually is identified as vibrations of C-O bounding that could be attributed to C-O bounding or also due to atmospheric CO_2 adsorbed in the surface.

Surface oxidation states were studied by XPS technique. Fig. 2 depicts the high resolution spectra of O 1s peak for the different synthesized solids. For graphene material compounds, the following surface oxygenated species have been considered [57]: oxide state typically recorded in oxides (~530 eV), O-C=O bounding (~531 eV), C=O groups (~532 eV), C-OH (~533eV) and C-O-C binding (~534 eV). In titania and magnetite, hydroxylated groups were detected at around 532 eV. Raw graphene was characterized by the presence of hydroxylated and carbonyl group, and very low proportion of carboxylic groups. Magnetic graphene (MG) presented higher proportion of carboxylic groups than graphene, probably due to a slight oxidation during the synthesis process. The incorporation of titania, with a low proportion of hydroxylated groups (i.e. around 5.6% of total oxygen) and MG support, led the enrichment of oxygenated groups. Actually, 10-MG-Ti fresh catalyst had 9.4% of carbonyl group (C=O) and 19.6% of

hydroxylated groups. After the 5th use of the catalyst an important decrease of oxygenated groups was recorded (only 10.7% of carbonyl group).

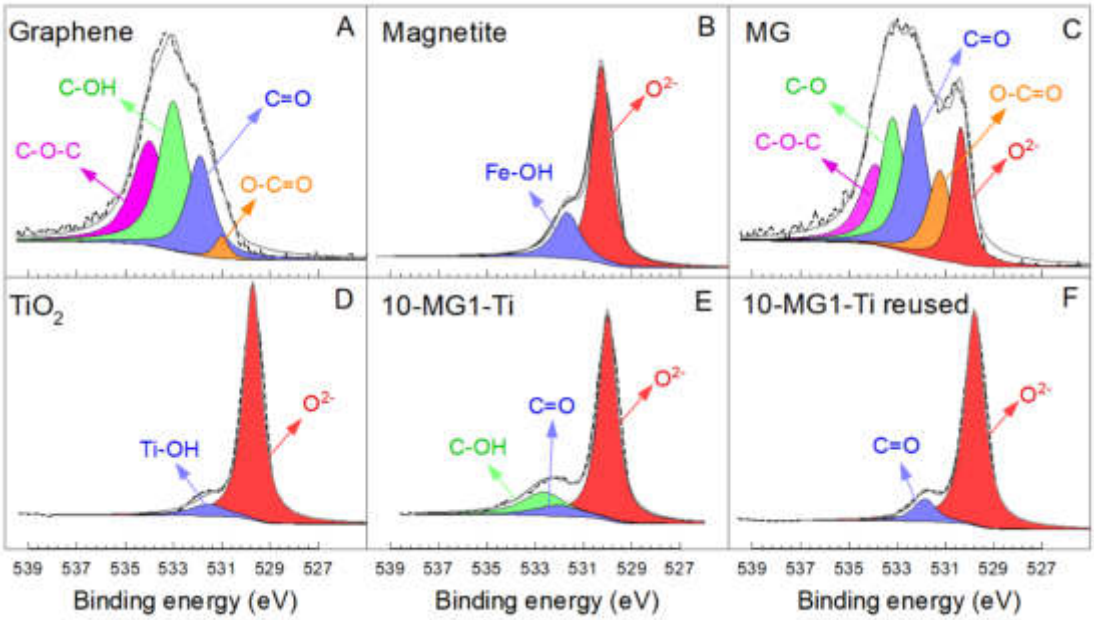

Figure 2. High resolution XPS survey for O 1s region of graphene (A), magnetite (B), magnetic graphene MG (C), bare TiO_2 (D), 10-MG1-Ti (E) and reused 10-MG1-Ti photocatalysts (F).

Optical properties of Y-MGX-Ti photocatalysts were studied by DR-UV-vis spectroscopy. Band gap was determined by Tauc's plot method (see Table 2 and Fig. S4). The presence of graphene oxide [33] or reduced graphene oxide in titania has been reported as a good strategy to reduce the band gap of photocatalysts [58] and, therefore, to enhance the activity in the visible region of the solar spectrum. The lab-made photocatalysts presented absorption of radiation up to 340 nm (see Fig. S4A). The determined bandgap for bare TiO_2 was 3.19 eV while the addition of magnetic graphene led to lower values in the range of 2.59-2.74 eV. However, the presence of graphene did not improve the performance of the degradation rate of cotinine with the simulated solar radiation (300-800 nm). Experiments filtering the radiation source to the visible region, i.e. 390-800 nm (results not shown), did not change this behavior, that means better

activity of graphene-based materials if compared to bare titania. A plausible explanation of this effect may be the higher recombination of the photo-induced species as graphene was used as support for titania and magnetite, and not as dopant agent to enhance photocatalytic activity [58].

Magnetic properties were analyzed by means of SQUID technique. Fig. 3 shows the results of magnetization of the synthesized photocatalysts. The magnetic moment, M_s, increased according to the proportion of magnetite. Actually, the maximum value was recorded for raw magnetite, M_s=70 emu g^{-1} (Fig. 3B). Although M_s values depend also on the magnetite particle size, values within 60-70 emu g^{-1} are frequently reported for magnetite nanoparticles. A plot of M_s *versus* the amount all iron, expressed as magnetite, in each sample led to a linear plot, see Fig. 3C, which confirms the presence of magnetite. Magnetite can undergo oxidation to the less magnetic maghemite (γ-Fe_3O_2). Nevertheless, it was not the case during the synthesis process of the lab made photocatalysts. The M_s values obtained matched the expected ones according to the M_s recorded for pure magnetite and the calculated amount of iron from WDRF analysis, considering all the presented iron as magnetite. The M_s for the solid 10-MG1-Ti was 2.74 emu g^{-1}. Similar values have been reported as suitable for photocatalytic ozonation treatment [25,26,59]. Although higher percentages of magnetite enhance the separation by increasing M_s, the photocatalytic activity would be reduced as it is shown in next section.

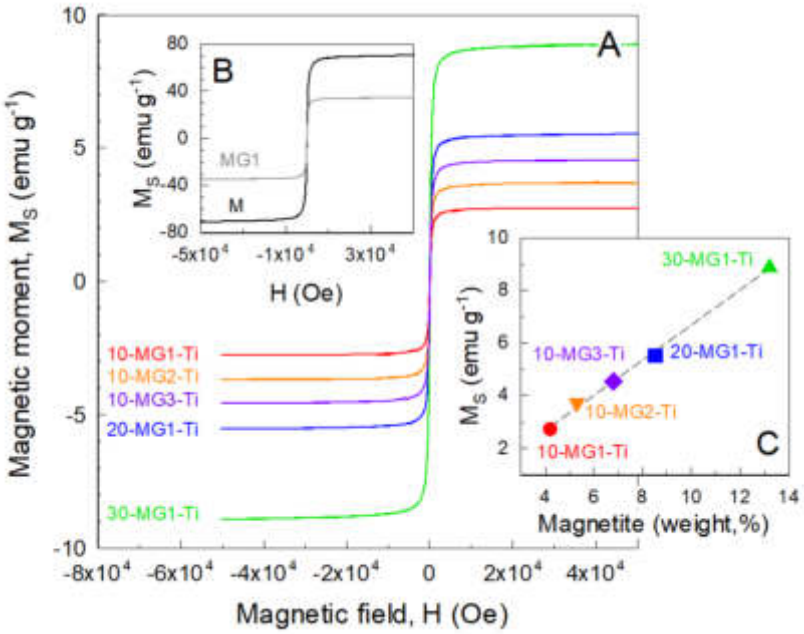

Figure 3. Magnetic moment (M_s) *versus* applied magnetic field (H). Figure A, magnetization in graphene-based TiO_2 photocatalysts. Figure B, magnetization of magnetite (M) and magnetic graphene (MG1). Figure C, magnetic moment *vs.* magnetite composition in graphene-based TiO_2 photocatalysts

3.2. Efficiency of photocatalytic ozonation with 10-MG1-Ti. Comparison to simpler technologies

A series of experiments to assess the efficiency on the removal of cotinine (CTN) as target pollutant were first carried out. Different technologies involving solar simulated radiation, ozone and the 10-MG1-Ti photocatalytic solid, selected in a first approach, were accomplished. Results are depicted in Fig. 4.

Although adsorption onto graphene has been reported in literature for a wide range of aqueous organic pollutants, even at low graphene dose [43]; no adsorption of cotinine was appreciated using 10-MG1-TiO_2 whose percentage of graphene is, theoretically, 5% of total. Photolysis produced negligible effect in the removal of the compound, i.e. less than 10% removal, as it could be deduced from its absorption UV-vis spectrum (no radiation absorption over 290 nm).

Photocatalysis is a well-known oxidative process in which Reactive Oxygen Species (ROS), mainly $HO^{\bullet}$, are generated due to the photo-activation of a semiconductor. The photocatalysis with 10-MG1-Ti in presence of oxygen was not capable of generate enough oxidative species to produce an efficient oxidation of the target pollutant (30% of cotinine removal). Consequently, more oxidative systems adding ozone were assessed.

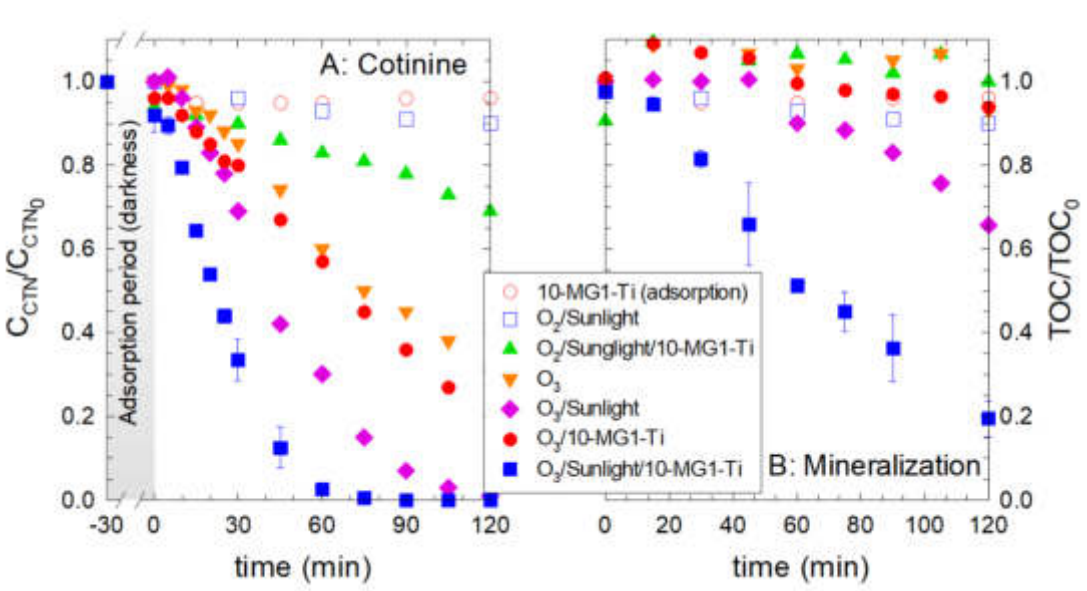

Figure 4. Comparison of different technologies combining simulated sunlight, ozone and the photocatalyst 10-MG1-Ti in the oxidation (A) and mineralization (B) of cotinine (CTN). Experimental conditions: V=500 mL; pH=free (initially 5.7±0.4); Q_{GAS}=30 L h^{-1}; $C_{O3inlet}$=10 mg L^{-1} (if required); $C_{10\text{-}MG1\text{-}Ti}$= 0.5 g L^{-1} (if required); $C_{CTN,0}$=10 mg L^{-1}.

Cotinine is a recalcitrant-to-oxidation organic with very low reactivity towards molecular ozone [44]. Actually, the second-order rate constant is estimated between 0.5-3.8 $M^{-1}s^{-1}$ in a pH range within 4-9 [45]. That is the reason why hydroxyl radical plays an important role in ozone-based systems for this kind of recalcitrant organic [44]. As can be appreciated in Fig. 4, single ozonation was capable to remove almost 70% of CTN in 2 hours under the experimental conditions tested. However, no mineralization was observed. Catalytic ozonation (O_3+10-MG1-Ti) poorly improved the results (removal *circa* 80% in 2 h). In fact, poor enhancement on the organic micropollutant is usually

registered in catalytic ozonation using titania [26,46,47]. When combining ozone and radiation, higher efficiencies in the degradation of CTN were observed. A complete degradation of cotinine was observed after 75 min of photocatalytic ozonation (radiation >300 nm). Furthermore, this technology demonstrated to be the most efficient not only in the oxidation rate and extent of CTN, but also in the mineralization extent reached that was almost 80% in 2 hours of treatment. Photolytic ozonation reached 30% of TOC removal whereas the rest of oxidative systems were inefficient to further oxidize the generated byproducts. The mineralization extent registered during photocatalytic ozonation (80% of TOC elimination), suggests important oxidation of intermediates and final oxidation organic acids.

Monitoring released organic acids, i.e. oxalic and formic acid, and nitrate (structure of cotinine contains 2 N atoms) gave evidence of the efficiency of oxidation of the final products (see Fig. 5). Single ozonation led to a constant release of nitrate and formic and oxalic acids, this later inhibited during the first hour of oxidation. Only formic acid was released during catalytic ozonation. The combination of ozone and radiation improved the release of formic acid and oxalic acid, diminishing also the inhibition period to 30 min. The application of photocatalytic ozonation was the most efficient process with the highest release of nitrate (approximately 35% of the total expected from the N contained in CTN molecule). It should be highlighted that no oxalic acid was registered during this process, the profile of formic acid reached a maximum at 30 min and decreased as the oxidation proceeded. Photocatalytic ozonation has been frequently reported as the most efficient system for the removal of short organic acids if compared to other simpler technologies involving ozone, radiation and photocatalysis [48].

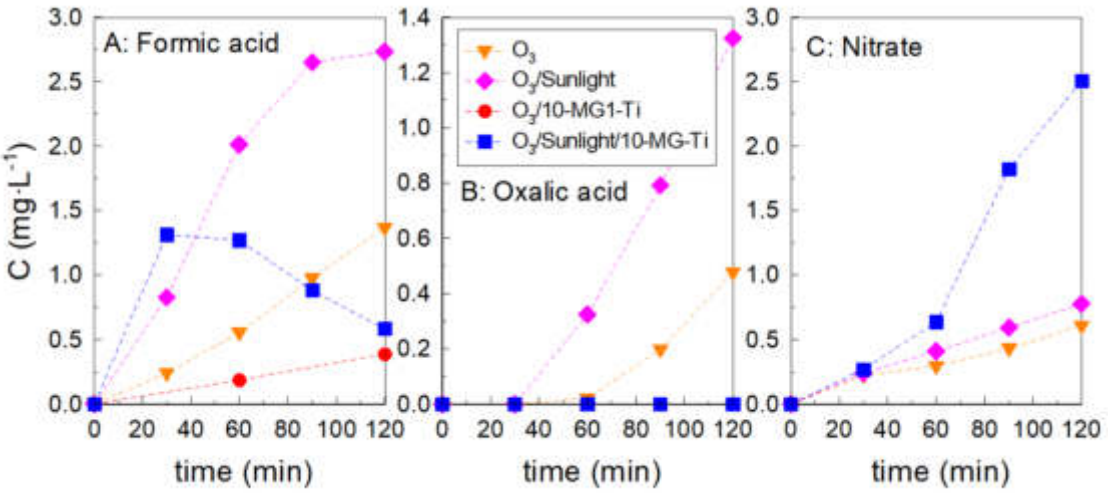

Figure 5. Evolution of the released formic acid (A), oxalic acid (B) and nitrate (C) during the oxidation of cotinine by means of different technologies combining simulated sunlight, ozone and the photocatalyst 10-MG1-Ti. Experimental conditions as shown in Fig. 1

The kinetic depletion of organic compounds in ozone-based systems can be described as a second-order irreversible reaction with molecular ozone and $HO^{\bullet}$ as the main oxidative specie, which could be simplified to a pseudo-first order kinetics. The molar balance of a target pollutant i in the perfectly mixed semibatch photoreactor used is:

$$-\frac{dC_i}{dt} = (k_{HO^{\bullet},i} C_{HO^{\bullet}} + k_{O_3,i} C_{O_3,dis}) C_i \approx k_{Obs} C_i \quad (1)$$

where C_i, $C_{HO^{\bullet}}$ and $C_{O3,dis}$ stand for the concentration of the target pollutant, hydroxyl radical and dissolved ozone, respectively; $k_{HO^{\bullet},i}$ and k_{O3} are the respective second-order rate constant of the reaction of the target pollutant with hydroxyl radical and molecular ozone; and k_{Obs} the pseudo-first order rate constant of the process.

The presence of radiation or catalysts in ozonation involves extra promotion routes for the generation of multiple ROS, primarily $HO^{\bullet}$ [49,50]. Direct reaction of CTN with molecular ozone can be disregarded and the contribution of photolysis with the radiation used is negligible (see Fig. 4). Therefore, it can be considered that CTN is exclusively

oxidized by the action of hydroxyl radicals. Thus, different tools can be used to evaluate the ability of each technology to decompose dissolved ozone into hydroxyl radicals.

The representation of the $HO^{\bullet}$ exposure *versus* time provides information about the evolution of the concentration of $HO^{\bullet}$. The exposure $HO^{\bullet}$ can be estimated by the following expression:

$$\int C_{HO^{\bullet}}.dt = \frac{\ln\left(C_{i_0}/C_i\right)}{k_{HO^{\bullet},i}} \quad (2)$$

The temporal evolution of $HO^{\bullet}$ concentration can be calculated by numerical derivation of the represented curve for Eq. 2.

Fig. 6 depicts the $HO^{\bullet}$ exposure *vs* time for the tested technologies. As observed, the combination of photocatalysis and ozone improved the production of hydroxyl radical if compared to catalytic or photolytic ozonation. Fig.6B proves the synergistic effect of photocatalytic ozonation process which cannot be explained by the contribution of simpler technologies, i.e. photolytic ozonation and catalytic ozonation (see dashed grey line in Fig. 6).

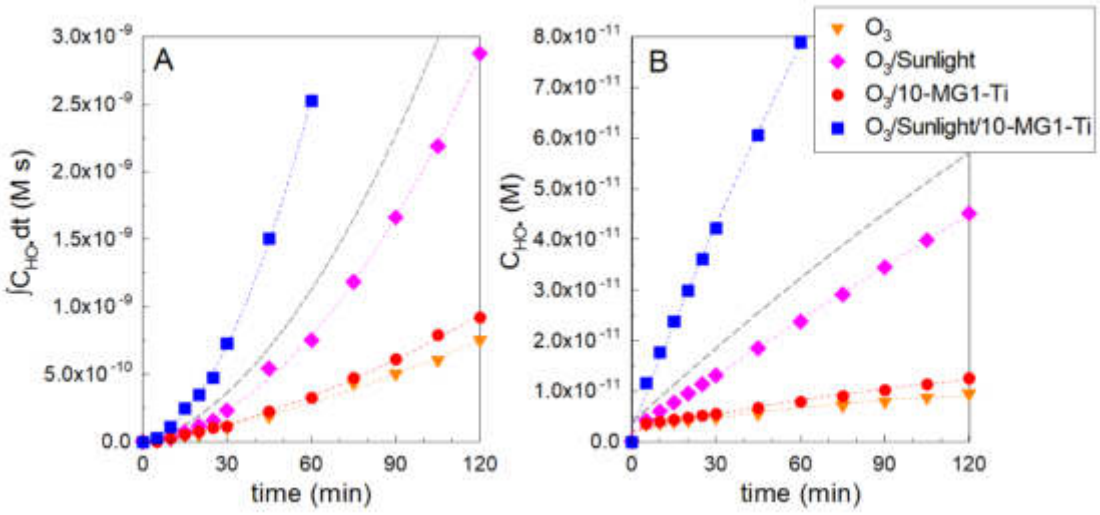

Figure 6. Evolution with time of the hydroxyl radical exposure (A) and concentration (B) for different technologies combining simulated sunlight, ozone and the photocatalyst 10-MG1-Ti. Experimental conditions as shown in Fig. 4. Dashed grey line: sum of photolytic and catalytic ozonation

The yield of $HO^\bullet$ production respect to the dissolved ozone exposure can be estimated by calculating the hydroxyl radical ratio to dissolve ozone through the R_{CT} concept [51]:

$$R_{CT} = \frac{\int C_{HO^\bullet} dt}{\int C_{O_3,dis} dt} = \frac{1}{k_{HO^\bullet,i}} \left(\frac{\ln\left(C_{i_0}/C_i\right)}{\int C_{O_3,dis} dt} - k_{O_3,i} \right) \approx \frac{\ln\left(C_{i_0}/C_i\right)}{k_{HO^\bullet,i} \int C_{O_3,dis} dt} \quad (3)$$

Eq. 3 is usually simplified disregarding the direct reaction between the organic pollutant and molecular ozone if the second-order rate constant for the direct reaction is low or negligible, which is the case of CTN. Monitoring the concentration of dissolved ozone *versus* time, it is possible to deduce the R_{CT} value from Eq. 3 by quantifying the ozone exposure numerically.

From Fig. 7A, a variation of R_{CT} values in two phases during photolytic, photocatalytic, and in minor extent, catalytic ozonation can be observed. The variation of R_{CT} has been frequently reported due to changes in initial O_3 dose, pH, temperature, alkalinity, presence of organic matter, etc. No changes in R_{CT} where registered during the

use of ozone alone. As shown in Table 3, R_{CT} values follows the order photocatalytic ozonation>> photolytic ozonation> catalytic ozonation~ single ozonation. This behavior also provides evidence of a higher production of hydroxyl radical during photocatalytic ozonation. Actually, if compared to single ozonation, photocatalytic ozonation registered 13-38 folded R_{CT}, during the first and second stage respectively.

Alternatively to R_{CT} parameter, a new concept was proposed by Kwon et al. [52] as the exposure of hydroxyl radical per O_3 consumed (Transferred Ozone Dose, TOD), $R_{HO\bullet,O3}$, that can be quantified for compounds that reacts slow with molecular ozone as:

$$R_{HO^\bullet,O_3} = \frac{\int C_{HO^\bullet} dt}{TOD} \approx \frac{\ln\left(C_{i_0}/C_i\right)}{k_{HO^\bullet,i} TOD} \quad (4)$$

Transferred Ozone Dose (TOD) stands the ozone consumption, understood as the ozone that is transferred to the liquid bulk per unit of volume and time:

$$TOD = \frac{1}{V}\int \left(F_{O_3,inlet} - F_{O_3,outlet}\right) dt = \frac{Q_{GAS}}{V}\int \left(C_{O_3,inlet} - C_{O_3,outlet}\right) dt \quad (5)$$

where V is the liquid of the semi-batch reactor, F_{O3} means the molar flow rate in the inlet or outlet of the reactor (respectively), Q_{GAS} is the volumetric flow rate of the O_2-O_3 gas mixture and C_{O3} the O_3 concentration in the gas phase. A monitoring of the concentration of the ozone concentration before and after passing the liquid phase allows to quantify the accumulated TOD by resolving Eq. 5 numerically.

$R_{HO\bullet,O3}$ was proposed as an alternative to R_{CT} to model ozonation process in one unique stage, in an attempt of avoiding the determination of the time in which R_{CT} changes, which strongly depends on the operational conditions and design of the setup [52]. However, as recently reported by Cruz-Alcalde et al. [53], the graphical representation of Eq. 4 (see Fig. 7B and 7B') led to 2 clearly differentiated stages of $R_{HO\bullet,O3}$ during photolytic and

photocatalytic ozonation, repeating the behavior observed in R_{CT}. Considering the physical meaning of this concept, $R_{HO\bullet,O3}$ informs about the production of hydroxyl radical per unit of ozone consumed according to a mass balance in the gas phase. From a system comparison, photocatalytic ozonation demonstrated to be an enhanced oxidation technology if compared to the simpler photolytic, catalytic or single ozonation. Table 3 summarizes the different values appreciated for all the systems in their two stages, or just one. The application of photocatalytic ozonation led to 3.3-7.6 times higher $R_{HO\bullet,O3}$ if compared to single ozonation. The second most efficient system, photolytic ozonation, improved folded $R_{HO\bullet,O3}$ parameter 1.9-5.6 times if compared to single ozonation.

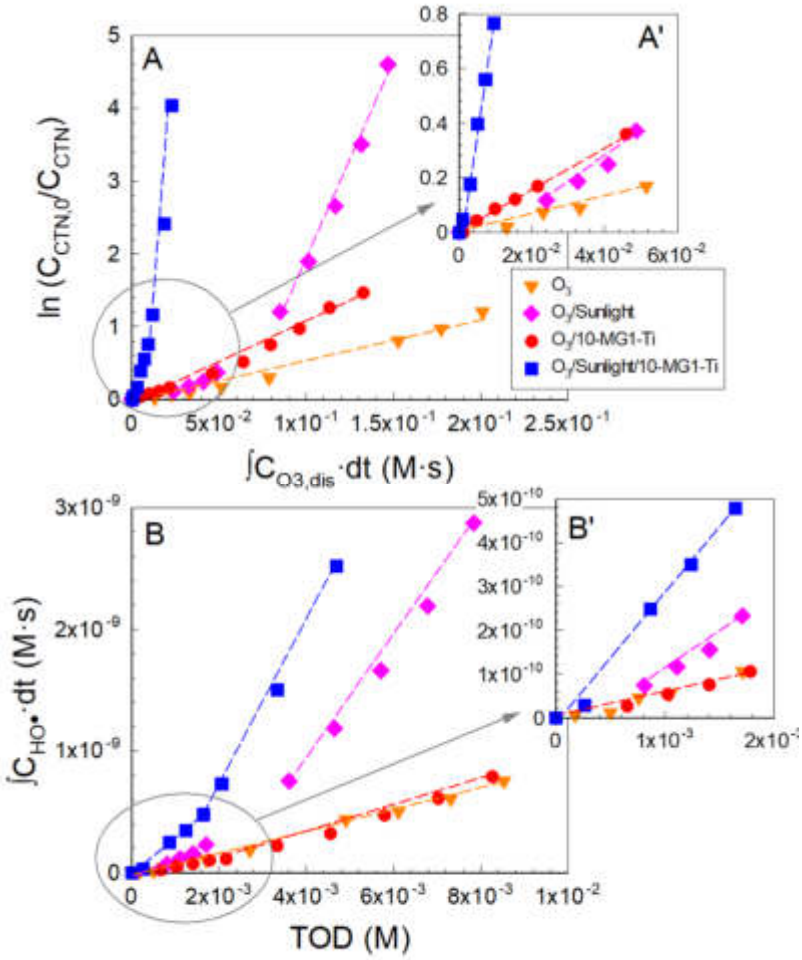

Figure 7. Graphical representation of R_{CT} (A) and $R_{HO\bullet,O3}$ (B) values according to Eqs. 3 and 4, respectively, during different ozone-based oxidation systems for cotinine abatement. Experimental conditions as shown in Fig. 4

Table 3 also includes the parameter η, defined as the ratio of the hydroxyl radical rate *versus* the direct reaction rate:

$$\eta = \frac{k_{HO^{\bullet},i} C_{HO^{\bullet}} C_i}{k_{O_3,i} C_{O_3} C_i} = \frac{k_{HO^{\bullet},i}}{k_{O_3,i}} R_{CT} \quad (6)$$

The second-order rate constant for the reaction of cotinine with hydroxyl radical and molecular ozone were respectively $1.6 \cdot 10^9$ $M^{-1}s^{-1}$ and 1.282 $M^{-1}s^{-1}$ at pH=6, according to a previous work [45].

Table 3. Photocatalytic (10-MG1-Ti) ozonation derived systems. Modelled parameters of the processes: k_{Obs}, R_{CT}, $R_{HO^{\bullet},O3}$ and η

System	k_{Obs}, h^{-1} (R^2)	R_{CT} (R^2)		$R_{HO^{\bullet},O3}$, s (R^2)		η
		1st phase	2nd phase	1st phase	2nd phase	
Photocatalysis (O_2/Sunlight/10-MG1-Ti)	0.126 (0.997)	- - -		- - -		- - -
Single ozonation (O_3)	0.595 (0.993)	$3.88 \cdot 10^{-9}$ (0.99)		$8.85 \cdot 10^{-8}$ (0.99)		4.61
Catalytic ozonation (O_3/10-MG1-Ti)	0.596 (0.999)	$4.43 \cdot 10^{-9}$ (0.97)	$8.38 \cdot 10^{-9}$ (0.99)	$9.86 \cdot 10^{-8}$ (0.98)		9.20
Photolytic ozonation (O_3/Sunlight)	1.031 (0.996)	$3.73 \cdot 10^{-9}$ (0.98)	$3.71 \cdot 10^{-8}$ (0.99)	$1.73 \cdot 10^{-7}$ (0.97)	$4.96 \cdot 10^{-7}$ (0.99)	38.4
Photocatalytic ozonation (O_3/Sunlight/10-MG1-Ti)	2.356 (0.998)	$5.14 \cdot 10^{-8}$ (0.99)	$1.47 \cdot 10^{-7}$ (0.97)	$2.99 \cdot 10^{-7}$ (0.96)	$6.69 \cdot 10^{-7}$ (0.99)	63.3

From the results in Table 3 it can be observed that ozone-based processes are stronger oxidation systems than photocatalysis by itself, with photocatalytic ozonation as the most efficient process. In fact, the pseudo-first order rate constant of photocatalytic ozonation was almost 17-folded if compared to photocatalysis, or 8 times higher than single ozonation. The sum of this two processes does no explain the higher k_{Obs} value obtained for the combined technology. A synergism [54] of almost 70% is appreciated. Furthermore, the R_{CT} and $R_{HO^{\bullet},O3}$ values also evidenced the higher production of $HO^{\bullet}$ in the order photocatalytic ozonation>photolytic ozonation>catalytic ozonation~ozonation.

Finally, the assessment of the importance of radical pathway (η) also evidenced a considerably higher importance of $HO^{\bullet}$ in photolytic and, specially, photocatalytic ozonation process. Consequently, photocatalytic ozonation process was selected as technology for further research.

3.3. Photocatalytic ozonation with Y-MGX-Ti. Influence of titania and graphene/magnetite ratio in the activity

The influence of titania percentage (100-Y), considering the support MG1 (weight ratio magnetite:graphene 1:1), was first evaluated. Different percentages of titania MG1 were selected, in order to increase the magnetite content and, therefore, to improve the separation properties of the initial selected 10-MG1-Ti. Also, for comparison purposes a non-magnetic TiO_2, synthesized following the same procedure, was included. Fig. 8 depicts the evolution with time of CTN normalized concentration and mineralization.

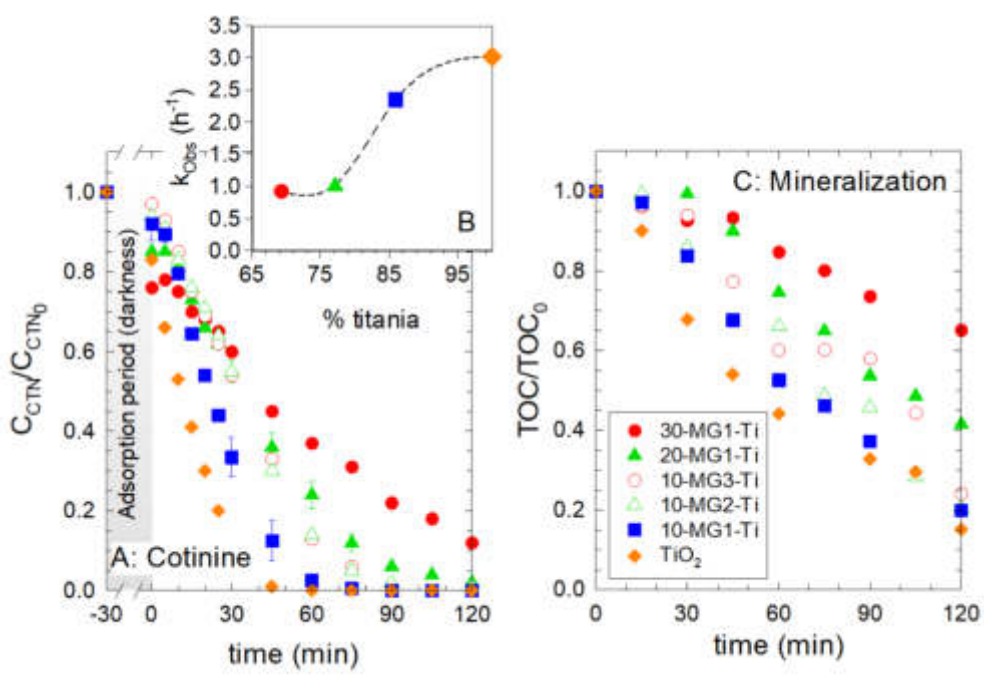

Figure 8. Titania and magnetite ratio influence on the photocatalytic ozonation of cotinine (CTN) using Y-MGX-Ti photocatalysts. Normalized evolution of cotinine (A), observed pseudo-first order rate constant *vs* the proportion of titania in the solid (B) and mineralization evolution (C). Experimental conditions: V=500 mL; pH=free (initially

5.8±0.5); Q_{GAS}=30 L h^{-1}; $C_{O3inlet}$=10 mg L^{-1}; $C_{photocatalyst}$= 0.5 g L^{-1} (0.4 g L^{-1} for TiO_2 series); $C_{CTN,0}$=10 mg L^{-1}.

As observed in Fig. 8, TiO_2 is the active species responsible for the photocatalytic activity. An analysis of the k_{Obs} versus the amount of titania present in the solid, according to the characterization results presented in the next section, gives evidence of this behavior. The higher amount of TiO_2, the better kinetic rate performance of CTN removal. The k_{Obs}, R_{CT}, $R_{HO•,O3}$ and importance of hydroxyl radical pathway (η) were assessed for the different photocatalytic solids (see Table 4). In comparison with the non-magnetic photocatalyst, the decrease of titania using MG1 support reduced the photocatalytic activity of the solid. On the other hand, when the percentage of titania was fixed to 90%, and the ratio of magnetite:graphene increased to 2:1 and 3:1 in the support, a negative effect was also registered. However, the photocatalyst 10-MG1-Ti performed acceptable photocatalytic results with still high recovery when applying an external magnetic field. Higher percentages of titania in MG1 were discarded due to the poor magnetic properties, which negatively impacted in the separation ability. Mineralization efficiency was also proportional to the amount of titania in the photocatalysts. Actually, the following mineralization efficiency was monitored: bare TiO_2> 10-MG1-Ti> 20-MG1-Ti> 30-MG1-Ti.

Table 4. Photocatalytic ozonation of CTN with Y-MGX-Ti: k_{Obs}, R_{CT} ratio and η

Photocatalyst	**k_{Obs}, h^{-1} (R^2)**	**R_{CT} (R^2)**		**$R_{HO•,O3}$, s (R^2)**		**η**
		1st phase	**2nd phase**	**1st phase**	**2nd phase**	
10-MG1-Ti	2.356 (0.998)	$5.14\cdot10^{-8}$ (0.99)	$1.47\cdot10^{-7}$ (0.97)	$2.99\cdot10^{-7}$ (0.96)	$6.69\cdot10^{-7}$ (0.99)	63.3
20-MG1-Ti	1.003 (0.999)	$3.06\cdot10^{-8}$ (0.99)	$5.31\cdot10^{-8}$ (0.99)	$2.40\cdot10^{-7}$ (0.99)		26.8
30-MG1-Ti	0.928 (0.995)	$1.36\cdot10^{-8}$ (0.9)	$2.60\cdot10^{-8}$ (0.99)	$1.21\cdot10^{-7}$ (0.99)		19.0
10-MG2-Ti	1.018 (0.997)	$2.49\cdot10^{-8}$ (0.99)	$6.91\cdot10^{-8}$ (0.97)	$1.80\cdot10^{-7}$ (0.98)	$4.74\cdot10^{-7}$ (0.99)	31.1

10-MG3-Ti	1.334 (0.989)	$2.94 \cdot 10^{-8}$ (0.99)	$7.01 \cdot 10^{-8}$ (0.97)	$1.85 \cdot 10^{-7}$ (0.99)	$5.37 \cdot 10^{-7}$ (1.00)	38.2
TiO_2	3.018 (0.995)	$8.89 \cdot 10^{-8}$ (0.99)	$2.09 \cdot 10^{-7}$ (1.00)	$3.23 \cdot 10^{-7}$ (0.99)	$1.20 \cdot 10^{-6}$ (1.00)	108.8

3.4. Stability and reusability of the 10-MG1-Ti catalyst under photocatalytic ozonation process

The photocatalyst 10-MG1-Ti was selected due to the highest activity of all the magnetic solids for the photocatalytic ozonation process, and also because of the reasonable magnetic properties to be recovered after the application of an external magnetic field. The reusability and activity behavior after consecutive cycles was studied by recovering the solid with the help of a magnet. Fig. 9 (top) depicts the evolution of the normalized cotinine concentration in each run. Also the mineralization degree after 120 min of treatment was studied (see Fig. 9 down right). No activity loss was recorded after 5 runs of use. Cotinine was completely removed before 90 min in all cases. The evolution of k_{Obs} in each run shows no significant catalytic loss of the solid. 81±3% of mineralization degree was observed after 120 min of photocatalytic ozonation.

The leaching of iron was also studied by analyzing the concentration of total iron species in solution. Fig. S5 depicts the temporal evolution of total iron release at different pH values for different titania ratios. Also, a magnetic photocatalyst without graphene and 90% of titania was prepared to elucidate the influence of graphene on the iron release. Neither the fresh 10-MG-Ti photocatalyst nor after 5 times of reusing led to iron release up the limit of detection of the spectrophotometric method (50 μg L^{-1}), at pH values of 4, 7 or 9, was appreciated. In absence of graphene, the release of iron was higher to the limit of detection, 90-450 ppb in 2h depending on the pH. The release for this solid was lower at pH=4<pH=9<pH=7. Therefore, the presence of graphene minimized the release of iron improving the stability of the magnetic properties.

From the characterization analysis, it is appreciated an important loss of carbon after the 5th reuse, and consequently a reduction on the external surface (Table 2). In addition, the hydroxylated groups in surface where oxidized into carbonyl groups (see Fig. 2). However, this carbon loss did not affect the activity of the catalyst nor compromise the release of iron into the solution.

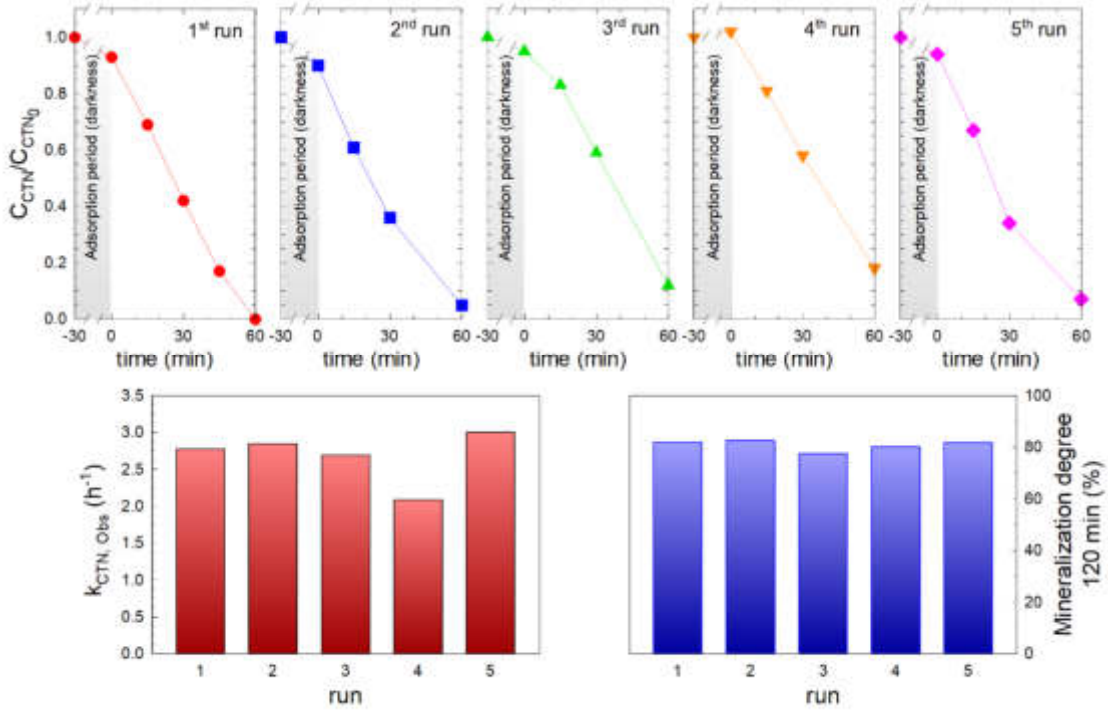

Figure 9. Stability study of 10-MG1-Ti under photocatalytic ozonation for the oxidation of cotinine. Experimental conditions: V=500 mL; pH=free (initially 6.2±0.3); Q_{GAS}=30 L h^{-1}; $C_{O3inlet}$=10 mg L^{-1}; $C_{10\text{-}MG1\text{-}Ti}$= 0.5 g L^{-1}; $C_{CTN,0}$=10 mg L^{-1}. Top, Evolution of remaining CTN normalized concentration during the recycling. Down left, pseudo-first order rate constant for CTN evolution. Down right, mineralization degree after 120 min.

3.5. A case of study: photocatalytic ozonation of a mixture of CECs in UWWTP matrix using magnetic 10-MG1-Ti

To further test the activity of the 10-MG1-Ti catalyst in a real scenario, an effluent of an urban wastewater treatment plant (UWWTP), was used as water matrix. A total of 10 micropollutants of emerging concern (CTN, cotinine; CAF, caffeine; CPR, ciprofloxacin;

MTP, metroprolol; SMX, sulfamethoxazole; DEET, N,N-Diethyl-m-toluamide; CLO, clofibric acid; BZF, bezafibrate; TSF, tritosulfuron; IBP, ibuprofen) were added at low concentration, i.e. 500 μg L^{-1}. Different scenarios (pH and removal of inorganic carbon, IC) were tested in order to evaluate the removal of the 10 CECs and the mineralization by means of ozonation, photolytic and photocatalytic ozonation technologies. Fig. 10 (left subfigures) depicts the observed pseudo-first order rate constant, $k_{Obs,i}$, for the different processes and compounds at pH=4 (Fig. 10A), the pH of the UWW effluent, that means ~8.4 (Fig. 10C) and after the removal of IC at the received pH (Fig. 10E). Also, the mineralization and oxalic acid concentration evolution are presented in Fig. 10 (right subfigures).

The rate constant k_{Obs} has been used as a mere tool for comparison purposes and depends on the operational conditions and UWW matrix in which tests were carried out. The behavior of the CECs under the three oxidative technologies can be grouped according to their reactivity towards molecular ozone. Generally, k_{Obs} values are closely related to the direct ozone rate constant (see Table S1). An increase of k_{Obs} was registered when applied photocatalytic ozonation for those compounds with low reactivity towards molecular ozone, i.e. direct rate constant with O_3 within the range 0.1-10 M^{-1} s^{-1}. This is the case of CTN, DEET, CLO, TSF and IBP. These compounds are eliminated via hydroxyl radical reaction; therefore, the application of radiation or photocatalysis improved, to a greater or lesser extent, their rate constant (k_{Obs}) as a higher production of $HO^{\bullet}$ took place. Compounds with a moderate value for the direct reaction with ozone, that means reactivity in the order of 100-1000 M^{-1} s^{-1}, are removed by both direct reactions with O_3 and free radical reactions [60], competing both theoretically in the process. This is the case of CAF, BZF and MTP. For those compounds the k_{Obs} during photocatalytic ozonation is slightly higher or similar to the registered one during single

ozonation or photolytic ozonation (excepting some particular case due to the complexity of the UWW matrix or errors in the operational conditions). Finally, SMX and CPR present high reactivity towards O_3 (rate constant $>10^3$ M^{-1} s^{-1}). For these two compounds photolytic and photocatalytic ozonation improved the value of k_{Obs} if compared to O_3, specially and surprisingly in the case of sulfamethoxazole at basic pH (rate constant with O_3 4.7-5.7 10^4 M^{-1} s^{-1}) if compared to O_3, even though the preferential reaction pathway is the reaction with molecular O_3.

pH affects considerably ozone-based AOPs since the anion HO^- catalyzes O_3 decomposition into $HO^{\bullet}$, minimizing the improvement of other radical pathway promoters such as light or catalysts. If the results at pH=4 and pH~8.4 are compared (Fig. 10A and E); in general terms, k_{Obs} for single ozonation is lower at acidic conditions. Some compounds have a radical change with pH due to the reactivity of the dissociated and non-dissociates species towards molecular ozone. This is the case of ciprofloxacin. This compound is highly reactive to O_3 ($>10^4$ M^{-1} s^{-1}) at basic pH but moderately reactive at acidic conditions (400 M^{-1} s^{-1}) [61]. This fact explains why the k_{Obs} was discreetly lower at pH=4 in the three systems applied.

Carbonates, which are a well-known $HO^{\bullet}$ scavenger [62], were removed by stripping with phosphoric acid, air bubbling and pH was restored to the UWW received value. As shown in Fig. 10C and 10E, the presence of inorganic carbon does not necessarily mean a negative effect in terms of contaminants removal rate. Only in the case of DEET, CLO acid BZF and IBP the removal of IC content was translated into higher k_{Obs} values, regarding the technology applied (photocatalytic, photolytic or single ozonation).

By analyzing the evolution of TOC and oxalic acid, different behavior was observed with the different technologies at the conditions analyzed. Thus, photocatalytic ozonation was the most efficient of all the technologies, especially at pH=4, as 70% of TOC removal

was reached in 2h. At the natural pH of the UWW effluent only 40% of mineralization after 2h was recorded and no differences between the addition or not of radiation is observed. From all the organic acids released during the oxidative treatments; i.e. formic, acetic, pyruvic, succinic and oxalic acid, the evolution of oxalic acid concentration deserves special attention since this organic is recalcitrant to the direct reaction with molecular ozone (<0.04 M^{-1} s^{-1} [63]). At the natural pH of the UWW effluent (~8.4), photocatalytic ozonation lead to the highest release of oxalic acid. Besides, if the total amount of TOC regarding the carboxylic acid detected is analyzed, photocatalytic ozonation led to a higher conversion of the TOC (not shown), which claims an enhancement in the effectiveness. It is noteworthy the lack of a really negative effect of IC in the formation of oxalic acid, as can be observed in Fig. 10D and 10F. Under acidic conditions, where the highest rate of mineralization was appreciated, oxalic acid was accumulated during single ozonation; however, photolytic and photocatalytic ozonation were capable to oxidize it after reaching a maximum in concentration.

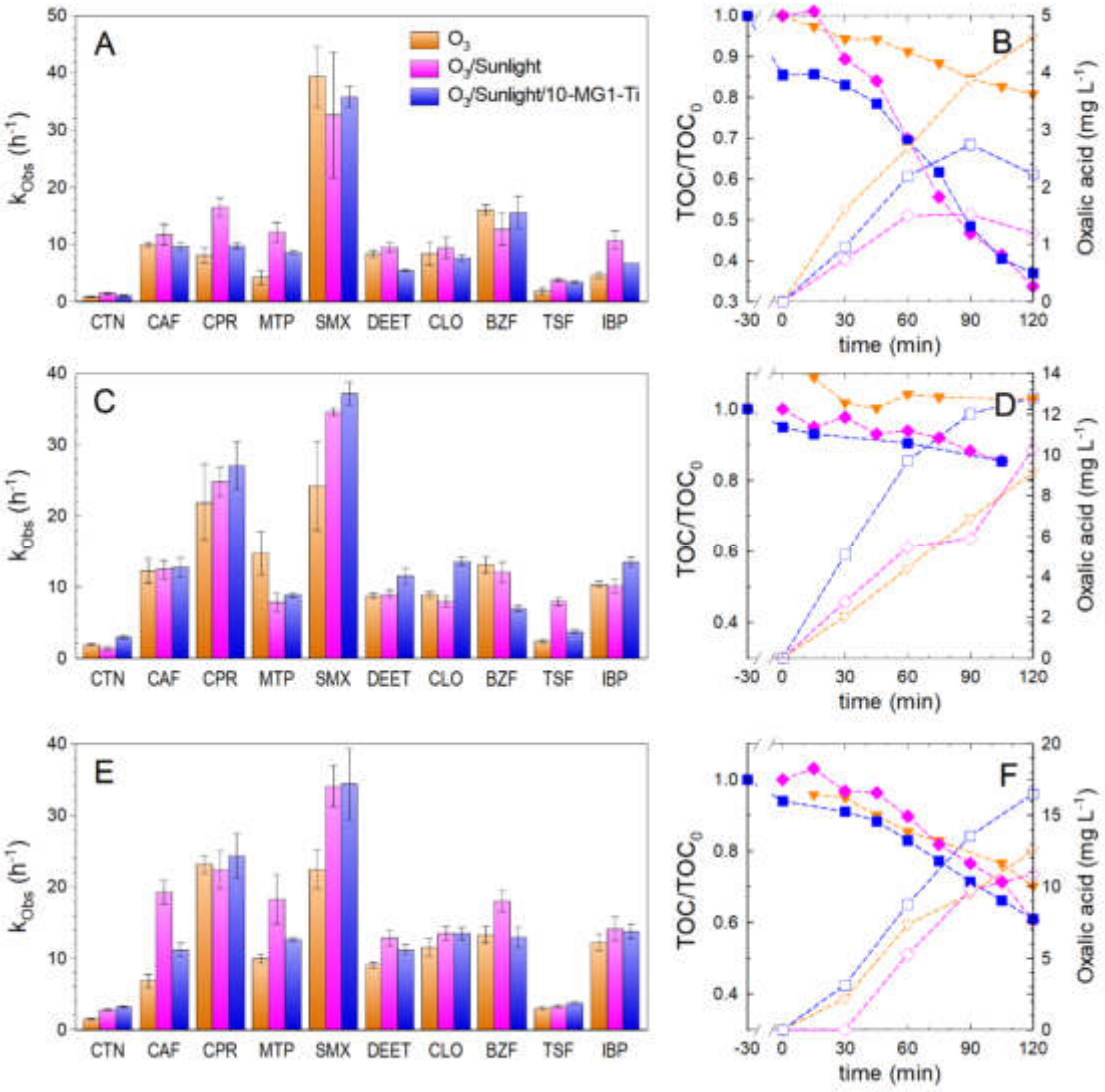

Figure 10. Ozonation, photolytic ozonation and photocatalytic ozonation of a mixture of 10 compounds in a secondary effluent of UWW. Experimental conditions: V=500 mL; Q_{GAS}=30 L h^{-1}; $C_{O3inlet}$=10 mg L^{-1}; $C_{10\text{-}MG1\text{-}Ti}$= 0.5 g L^{-1} (if required); $C_{CEC,0}$=500 µg L^{-1} (each); H_3PO_4= 6 mM (if required). Pseudo-first order rate constant for the degradation of each contaminant at pH=4 (A), natural pH with inorganic carbon (C) and natural pH without inorganic carbon (E). Mineralization (filled symbols) and evolution of oxalic (open symbols) acid at pH=4 (B), natural pH with inorganic carbon (D) and natural pH without inorganic carbon (F).

4. CONCLUSIONS

Commercial graphene was successfully applied as a support for titania and magnetite particles with high photocatalytic activity in presence of ozone and magnetic properties

for the solid separation after the treated aqueous solution. The photocatalytic ozonation process proved to be more efficient if compared to simpler technologies (photolytic, catalytic or single ozonation) applied to the degradation of a model pollutant recalcitrant to the direct reaction with molecular ozone, i.e. cotinine. From the analysis of diverse kinetic parameters ($HO^{\bullet}$ exposure *vs* time, R_{CT} and $R_{HO\bullet,O3}$ ratios), a synergistic effect in the production of hydroxyl radicals for the combination of ozone and photocatalysis was registered. The study of the influence of magnetic-graphene: titania ratio on the photocatalytic activity suggests that titania particles are responsible for the photocatalytic activity; with the highest activity registered in the case of bare titania.

Characterization of the solid proved the presence of titania and magnetite particles homogeneously distributed in the graphene surface, acting graphene as a carbonaceous support. Although the presence of magnetic graphene compromised the photoactivity of the solid (it was lower than bare titania), this loss in activity was balanced by the incorporation of magnetic properties that facilitate the recovery after the treatment. The attachment of magnetic particles in graphene remained stable enough after 5 reuses with no appreciable iron leaching in the solution and no significant loss of photocatalytic activity.

The study was extended to a real scenario for the oxidation of a mixture of 10 well-known micropollutants of emerging concern in a real water matrix from a local wastewater treatment plant. The application of photocatalytic ozonation with the magnetic graphene-based titania successfully oxidized the pollutants with an increase in the pseudo-first order rate constant of recalcitrant to ozonation compounds; and also the mineralization extent if compared to simpler technologies.

Acknowledgements

Authors thank to the MINECO *(Ministerio de Economía y Competitividad)* of Spain and European Funds for Regional Development for the economic support trough Project CTQ2015/64944-R. SACSS *(Servicio de Análisis y Caracterización de Sólidos y Superficies)* of SAIUEx at the Extremadura's University is also acknowledged for the catalysts' characterization guidance.

Ms. Ana María Chávez is also thankful to the Spanish MINECO for her predoctoral contract (call 2013). Mr. Rafael Rodríguez Solís is grateful to *Ramón Areces* foundation for his postdoctoral fellowship in the University of Cincinnati (XXX edition of grants for Postgraduate Studies in Life and Matter Sciences in Foreign Universities and Research Centers 2018/2019).

REFERENCES

[1] B. Petrie, R. Barden, B. Kasprzyk-Hordern, A review on emerging contaminants in wastewaters and the environment: Current knowledge, understudied areas and recommendations for future monitoring, Water Res. 72 (2015) 3–27. doi:10.1016/J.WATRES.2014.08.053.

[2] A. Gogoi, P. Mazumder, V.K. Tyagi, G.G. Tushara Chaminda, A.K. An, M. Kumar, Occurrence and fate of emerging contaminants in water environment: A review, Groundw. Sustain. Dev. 6 (2018) 169–180. doi:10.1016/J.GSD.2017.12.009.

[3] S. Fekadu, E. Alemayehu, R. Dewil, B. Van der Bruggen, Pharmaceuticals in freshwater aquatic environments: A comparison of the African and European challenge, Sci. Total Environ. 654 (2019) 324–337. doi:10.1016/J.SCITOTENV.2018.11.072.

[4] M. Gavrilescu, K. Demnerová, J. Aamand, S. Agathos, F. Fava, Emerging pollutants in the environment: present and future challenges in biomonitoring,

ecological risks and bioremediation, N. Biotechnol. 32 (2015) 147–156. doi:10.1016/J.NBT.2014.01.001.

[5] E. Nilsen, K.L. Smalling, L. Ahrens, M. Gros, K.S.B. Miglioranza, Y. Picó, H.L. Schoenfuss, Critical review: Grand challenges in assessing the adverse effects of contaminants of emerging concern on aquatic food webs, Environ. Toxicol. Chem. 38 (2019) 46–60. doi:10.1002/etc.4290.

[6] A. Zarei-Baygi, M. Harb, P. Wang, L.B. Stadler, A.L. Smith, Evaluating Antibiotic Resistance Gene Correlations with Antibiotic Exposure Conditions in Anaerobic Membrane Bioreactors, Environ. Sci. Technol. 5 (2019) 3599–360. doi:10.1021/acs.est.9b00798.

[7] A. Christou, A. Agüera, J.M. Bayona, E. Cytryn, V. Fotopoulos, D. Lambropoulou, C.M. Manaia, C. Michael, M. Revitt, P. Schröder, D. Fatta-Kassinos, The potential implications of reclaimed wastewater reuse for irrigation on the agricultural environment: The knowns and unknowns of the fate of antibiotics and antibiotic resistant bacteria and resistance genes – A review, Water Res. 123 (2017) 448–467. doi:10.1016/J.WATRES.2017.07.004.

[8] I. Michael, L. Rizzo, C.S. McArdell, C.M. Manaia, C. Merlin, T. Schwartz, C. Dagot, D. Fatta-Kassinos, Urban wastewater treatment plants as hotspots for the release of antibiotics in the environment: A review, Water Res. 47 (2013) 957–995. doi:10.1016/J.WATRES.2012.11.027.

[9] P. Krzeminski, M.C. Tomei, P. Karaolia, A. Langenhoff, C.M.R. Almeida, E. Felis, F. Gritten, H.R. Andersen, T. Fernandes, C.M. Manaia, L. Rizzo, D. Fatta-Kassinos, Performance of secondary wastewater treatment methods for the removal of contaminants of emerging concern implicated in crop uptake and antibiotic resistance spread: A review, Sci. Total Environ. 648 (2019) 1052–1081.

doi:10.1016/J.SCITOTENV.2018.08.130.

[10] A.R. Ribeiro, O.C. Nunes, M.F.R. Pereira, A.M.T. Silva, An overview on the advanced oxidation processes applied for the treatment of water pollutants defined in the recently launched Directive 2013/39/EU, Environ. Int. 75 (2015) 33–51. doi:10.1016/J.ENVINT.2014.10.027.

[11] I. Gültekin, N.H. Ince, Synthetic endocrine disruptors in the environment and water remediation by advanced oxidation processes, J. Environ. Manage. 85 (2007) 816–832. doi:10.1016/J.JENVMAN.2007.07.020.

[12] M.A. Oturan, J.-J. Aaron, Advanced Oxidation Processes in Water/Wastewater Treatment: Principles and Applications. A Review, Crit. Rev. Environ. Sci. Technol. 44 (2014) 2577–2641. doi:10.1080/10643389.2013.829765.

[13] I.C. Iakovides, I. Michael-Kordatou, N.F.F. Moreira, A.R. Ribeiro, T. Fernandes, M.F.R. Pereira, O.C. Nunes, C.M. Manaia, A.M.T. Silva, D. Fatta-Kassinos, Continuous ozonation of urban wastewater: Removal of antibiotics, antibiotic-resistant Escherichia coli and antibiotic resistance genes and phytotoxicity, Water Res. 159 (2019) 333–347. doi:10.1016/J.WATRES.2019.05.025.

[14] T.E. Agustina, H.M. Ang, V.K. Vareek, A review of synergistic effect of photocatalysis and ozonation on wastewater treatment, J. Photochem. Photobiol. C Photochem. Rev. 6 (2005) 264–273. doi:10.1016/J.JPHOTOCHEMREV.2005.12.003.

[15] V. Augugliaro, M. Litter, L. Palmisano, J. Soria, The combination of heterogeneous photocatalysis with chemical and physical operations: A tool for improving the photoprocess performance, J. Photochem. Photobiol. C Photochem. Rev. 7 (2006) 127–144. doi:10.1016/J.JPHOTOCHEMREV.2006.12.001.

[16] J.F. Beltrán, A. Rey, Solar or UVA-Visible Photocatalytic Ozonation of Water

Contaminants, Molecules. 22 (2017) 1177. doi:10.3390/molecules22071177.

[17] M. Mehrjouei, S. Müller, D. Möller, A review on photocatalytic ozonation used for the treatment of water and wastewater, Chem. Eng. J. 263 (2015) 209–219. doi:10.1016/J.CEJ.2014.10.112.

[18] J. Xiao, Y. Xie, H. Cao, Organic pollutants removal in wastewater by heterogeneous photocatalytic ozonation, Chemosphere. 121 (2015) 1–17. doi:10.1016/J.CHEMOSPHERE.2014.10.072.

[19] N. Serpone, Is the Band Gap of Pristine TiO2 Narrowed by Anion- and Cation-Doping of Titanium Dioxide in Second-Generation Photocatalysts?, J. Phys. Chem. B. 110 (2006) 24287–24293. doi:10.1021/JP065659R.

[20] E.M. Rodríguez, A. Rey, E. Mena, F.J. Beltrán, Application of solar photocatalytic ozonation in water treatment using supported TiO2, Appl. Catal. B Environ. 254 (2019) 237–245. doi:10.1016/J.APCATB.2019.04.095.

[21] M.A. Lazar, S. Varghese, S.S. Nair, Photocatalytic Water Treatment by Titanium Dioxide: Recent Updates, Catalysts. 2 (2012) 572–601. doi:10.3390/catal2040572.

[22] N.M. Mahmoodi, Photocatalytic ozonation of dyes using copper ferrite nanoparticle prepared by co-precipitation method, Desalination. 279 (2011) 332–337. doi:10.1016/J.DESAL.2011.06.027.

[23] N.M. Mahmoodi, M. Bashiri, S.J. Moeen, Synthesis of nickel–zinc ferrite magnetic nanoparticle and dye degradation using photocatalytic ozonation, Mater. Res. Bull. 47 (2012) 4403–4408. doi:10.1016/J.MATERRESBULL.2012.09.036.

[24] L. Ciccotti, L.A.S. do Vale, T.L.R. Hewer, R.S. Freire, Fe_3O_4@TiO_2 preparation and catalytic activity in heterogeneous photocatalytic and ozonation processes, Catal. Sci. Technol. 5 (2015) 1143–1152. doi:10.1039/C4CY01242A.

[25] A. Rey, D.H. Quiñones, P.M. Álvarez, F.J. Beltrán, P.K. Plucinski, Simulated

solar-light assisted photocatalytic ozonation of metoprolol over titania-coated magnetic activated carbon, Appl. Catal. B Environ. 111–112 (2012) 246–253. doi:10.1016/J.APCATB.2011.10.005.

[26] D.H. Quiñones, A. Rey, P.M. Álvarez, F.J. Beltrán, P.K. Plucinski, Enhanced activity and reusability of TiO2 loaded magnetic activated carbon for solar photocatalytic ozonation, Appl. Catal. B Environ. 144 (2014) 96–106. doi:10.1016/J.APCATB.2013.07.005.

[27] L. Yu, D. Wang, D. Ye, Solar photocatalytic ozonation of emerging contaminants detected in municipal wastewater treatment plant effluents by magnetic MWCNTs/TiO $_2$ nanocomposites, RSC Adv. 5 (2015) 96896–96904. doi:10.1039/C5RA18752D.

[28] P.M. Álvarez, D.H. Quiñones, I. Terrones, A. Rey, F.J. Beltrán, Insights into the removal of terbuthylazine from aqueous solution by several treatment methods, Water Res. 98 (2016) 334–343. doi:10.1016/J.WATRES.2016.04.026.

[29] S. Chowdhury, R. Balasubramanian, Recent advances in the use of graphene-family nanoadsorbents for removal of toxic pollutants from wastewater, Adv. Colloid Interface Sci. 204 (2014) 35–56. doi:10.1016/J.CIS.2013.12.005.

[30] J. Xiao, Y. Xie, H. Cao, Y. Wang, Z. Guo, Y. Chen, Towards effective design of active nanocarbon materials for integrating visible-light photocatalysis with ozonation, Carbon N. Y. 107 (2016) 658–666. doi:10.1016/J.CARBON.2016.06.066.

[31] G. Liao, D. Zhu, J. Zheng, J. Yin, B. Lan, L. Li, Efficient mineralization of bisphenol A by photocatalytic ozonation with TiO2–graphene hybrid, J. Taiwan Inst. Chem. Eng. 67 (2016) 300–305. doi:10.1016/J.JTICE.2016.07.035.

[32] M. Sheydaei, H.R.K. Shiadeh, B. Ayoubi-Feiz, R. Ezzati, Preparation of nano N-

TiO2/graphene oxide/titan grid sheets for visible light assisted photocatalytic ozonation of cefixime, Chem. Eng. J. 353 (2018) 138–146. doi:10.1016/J.CEJ.2018.07.089.

[33] M. Checa, M. Figueredo, A. Aguinaco, F.J. Beltrán, Graphene oxide/titania photocatalytic ozonation of primidone in a visible LED photoreactor, J. Hazard. Mater. 369 (2019) 70–78. doi:10.1016/J.JHAZMAT.2019.02.025.

[34] L. Lian, S. Yan, B. Yao, S.-A. Chan, W. Song, Photochemical Transformation of Nicotine in Wastewater Effluent, Environ. Sci. Technol. 51 (2017) 11718–11730. doi:10.1021/acs.est.7b03223.

[35] J. Chen, A.K. Venkatesan, R.U. Halden, Alcohol and nicotine consumption trends in three U.S. communities determined by wastewater-based epidemiology, Sci. Total Environ. 656 (2019) 174–183. doi:10.1016/J.SCITOTENV.2018.11.350.

[36] R. Kumar, B. Tscharke, J. O'Brien, J.F. Mueller, C. Wilkins, L.P. Padhye, Assessment of drugs of abuse in a wastewater treatment plant with parallel secondary wastewater treatment train, Sci. Total Environ. 658 (2019) 947–957. doi:10.1016/J.SCITOTENV.2018.12.167.

[37] J. Antonio Baz-Lomba, S. Salvatore, E. Gracia-Lor, R. Bade, S. Castiglioni, E. Castrignanò, A. Causanilles, F. Hernandez, B. Kasprzyk-Hordern, J. Kinyua, A.-K. Mccall, A. Van Nuijs, C. Ort, B.G. Plósz, P. Ramin, M. Reid, N.I. Rousis, Y. Ryu, P. De Voogt, J. Bramness, K. Thomas, Comparison of pharmaceutical, illicit drug, alcohol, nicotine and caffeine levels in wastewater with sale, seizure and consumption data for 8 European cities, BMC Public Health. 16 (2016) 1035. doi:10.1186/s12889-016-3686-5.

[38] M. Huerta-Fontela, M.T. Galceran, J. Martin-Alonso, F. Ventura, Occurrence of psychoactive stimulatory drugs in wastewaters in north-eastern Spain, Sci. Total

Environ. 397 (2008) 31–40. doi:10.1016/J.SCITOTENV.2008.02.057.

[39] M. Cao, P. Wang, Y. Ao, C. Wang, J. Hou, J. Qian, Photocatalytic degradation of tetrabromobisphenol A by a magnetically separable graphene–TiO2 composite photocatalyst: Mechanism and intermediates analysis, Chem. Eng. J. 264 (2015) 113–124. doi:10.1016/J.CEJ.2014.10.011.

[40] J. Tauc, Optical properties and electronic structure of amorphous Ge and Si, Mater. Res. Bull. 3 (1968) 37–46. doi:10.1016/0025-5408(68)90023-8.

[41] R.R. Solís, O. Gimeno, F.J. Rivas, F.J. Beltrán, Simulated solar driven photolytic ozonation for the oxidation of aqueous recalcitrant-to-ozone tritosulfuron. Transformation products and toxicity, J. Environ. Manage. 233 (2019) 513–522. doi:10.1016/J.JENVMAN.2018.12.068.

[42] H. Bader, J. Hoigné, Determination of ozone in water by the indigo method, Water Res. 15 (1981) 449–456. doi:10.1016/0043-1354(81)90054-3.

[43] G. Ersan, O.G. Apul, F. Perreault, T. Karanfil, Adsorption of organic contaminants by graphene nanosheets: A review, Water Res. 126 (2017) 385–398. doi:10.1016/J.WATRES.2017.08.010.

[44] R. Rosal, A. Rodríguez, J.A. Perdigón-Melón, A. Petre, E. García-Calvo, M.J. Gómez, A. Agüera, A.R. Fernández-Alba, Occurrence of emerging pollutants in urban wastewater and their removal through biological treatment followed by ozonation, Water Res. 44 (2010) 578–588. doi:10.1016/J.WATRES.2009.07.004.

[45] F.J. Rivas, R.R. Solís, F.J. Beltrán, O. Gimeno, Sunlight driven photolytic ozonation as an advanced oxidation process in the oxidation of bezafibrate, cotinine and iopamidol, Water Res. 151 (2019) 226–242. doi:10.1016/J.WATRES.2018.12.013.

[46] F.J. Beltrán, A. Aguinaco, J.F. García-Araya, A. Oropesa, Ozone and

photocatalytic processes to remove the antibiotic sulfamethoxazole from water, Water Res. 42 (2008) 3799–3808. doi:10.1016/J.WATRES.2008.07.019.

[47] R.R. Solís, F.J. Rivas, J.L. Pérez-Bote, O. Gimeno, Photocatalytic ozonation of 4-chloro-2-methylphenoxyacetic acid and its reaction intermediate 4-chloro-2-methyl phenol, J. Taiwan Inst. Chem. Eng. 46 (2015) 125–131. doi:10.1016/J.JTICE.2014.09.010.

[48] R.R. Solís, F.J. Rivas, A. Martínez-Piernas, A. Agüera, Ozonation, photocatalysis and photocatalytic ozonation of diuron: Intermediates identification, Chem. Eng. J. 292 (2016). doi:10.1016/j.cej.2016.02.005.

[49] G.R. Peyton, W.H. Glaze, Destruction of pollutants in water with ozone in combination with ultraviolet radiation. 3. Photolysis of aqueous ozone, Environ. Sci. Technol. 22 (1988) 761–767. doi:10.1021/es00172a003.

[50] J. Nawrocki, B. Kasprzyk-Hordern, The efficiency and mechanisms of catalytic ozonation, Appl. Catal. B Environ. 99 (2010) 27–42. doi:10.1016/J.APCATB.2010.06.033.

[51] M.S. Elovitz, U. von Gunten, Hydroxyl Radical/Ozone Ratios During Ozonation Processes. I. The R_{ct} Concept, Ozone Sci. Eng. 21 (1999) 239–260. doi:10.1080/01919519908547239.

[52] M. Kwon, H. Kye, Y. Jung, Y. Yoon, J.-W. Kang, Performance characterization and kinetic modeling of ozonation using a new method: ROH,O3 concept, Water Res. 122 (2017) 172–182. doi:10.1016/J.WATRES.2017.05.062.

[53] A. Cruz-Alcalde, S. Esplugas, C. Sans, Abatement of ozone-recalcitrant micropollutants during municipal wastewater ozonation: Kinetic modelling and surrogate-based control strategies, Chem. Eng. J. 360 (2019) 1092–1100. doi:10.1016/J.CEJ.2018.10.206.

[54] R.R. Solís, F.J. Rivas, O. Gimeno, J.L. Pérez-Bote, Photocatalytic ozonation of clopyralid, picloram and triclopyr. Kinetics, toxicity and influence of operational parameters, J. Chem. Technol. Biotechnol. 91 (2016) 51–58. doi:10.1002/jctb.4542.

[55] L. Escobar-Alarcón, M.E. Espinosa-Pesqueira, D.A. Solis-Casados, J. Gonzalo, J. Solis, M. Martinez-Orts, E. Haro-Poniatowski, Two-dimensional carbon nanostructures obtained by laser ablation in liquid: effect of an ultrasonic field, Appl. Phys. A. 124 (2018) 124–141. doi:10.1007/s00339-018-1559-8.

[56] Y. Hao, Y. Wang, L. Wang, Z. Ni, Z. Wang, R. Wang, C.K. Koo, Z. Shen, J.T.L. Thong, Probing Layer Number and Stacking Order of Few-Layer Graphene by Raman Spectroscopy, Small. 6 (2010) 195–200. doi:10.1002/smll.200901173.

[57] R. Al-Gaashani, A. Najjar, Y. Zakaria, S. Mansour, M.A. Atieh, XPS and structural studies of high quality graphene oxide and reduced graphene oxide prepared by different chemical oxidation methods, Ceram. Int. 45 (2019) 14439–14448. doi:10.1016/J.CERAMINT.2019.04.165.

[58] A. Tayel, A. Ramadan, O. El Seoud, A. Tayel, A.R. Ramadan, O.A. El Seoud, Titanium Dioxide/Graphene and Titanium Dioxide/Graphene Oxide Nanocomposites: Synthesis, Characterization and Photocatalytic Applications for Water Decontamination, Catalysts. 8 (2018) 491. doi:10.3390/catal8110491.

[59] L. de Oliveira Pereira, I. Marques Sales, L. Pereira Zampiere, S. Silveira Vieira, I. do Rosário Guimarães, F. Magalhães, Preparation of magnetic photocatalysts from TiO2, activated carbon and iron nitrate for environmental remediation, J. Photochem. Photobiol. A Chem. 382 (2019) 111907. doi:10.1016/J.JPHOTOCHEM.2019.111907.

[60] F.J. Beltrán, A. Rey, Free Radical and Direct Ozone Reaction Competition to

Remove Priority and Pharmaceutical Water Contaminants with Single and Hydrogen Peroxide Ozonation Systems, Ozone Sci. Eng. 40 (2018) 251–265. doi:10.1080/01919512.2018.1431521.

[61] M.C. Dodd, M.O. Buffle, U. Von Gunten, Oxidation of antibacterial molecules by aqueous ozone: moiety-specific reaction kinetics and application to ozone-based wastewater treatment, Environ. Sci. Technol. 40 (2006) 1969–1977. doi:10.1021/es051369x.

[62] J.L. Acero, U. von Gunten, Influence of Carbonate on the Ozone/Hydrogen Peroxide Based Advanced Oxidation Process for Drinking Water Treatment, Ozone Sci. Eng. 22 (2000) 305–328. doi:10.1080/01919510008547213.

[63] J. Hoigné, H. Bader, Rate constants of reactions of ozone with organic and inorganic compounds in water—II: Dissociating organic compounds, Water Res. 17 (1983) 185–194. doi:10.1016/0043-1354(83)90099-4.